Supplementary Information:

Table S1. Receiving fault parameters for the calculation of stress disturbance.
Figure S1. Checkerboard test for the inversion of the InSAR and GPS data.
Figure S2. Coseismic Coulomb stress changes with the receiving fault of the mainshock rupture (i.e., strike = 154°, dip = 77°, rake = –8°, friction = 0.1).
Figure S3. Coseismic Coulomb stress changes with the receiving fault of the mainshock rupture (i.e., strike = 154°, dip = 77°, rake = –8°, friction = 0.7).
Figure S4. The comparison of our slip distribution model with existing models.
Figure S5. Coseismic Coulomb stress changes caused by the different slip models with the receiving fault of the mainshock rupture (i.e., strike = 154°, dip = 77°, rake = –8°, friction = 0.4) at the depth of 15km.
Figure S6. Static Coulomb stress disturbances caused by the different slip models with the same receiving fault (Table S1) at the depth of 5 km.

Table S1. Receiving fault parameters for the calculation of stress disturbance.

Fault Name	**Strike / (°)**	**Dip / (°)**	**Rake / (°)**	**Friction**	**σ/MPa**
DW	290	75	45	0.5	(–0.0100, 0.0087)
EK	135	89	0	0.4	(–0.0004, –0.0001)
GA	225	45	90	0.7	(0.0000, 0.0001)
LD	300	60	15	0.6	(–0.0018, 0.0010)
LL	65	65	–45	0.6	(0.0000, 0.0005)
LRB	217	60	135	0.6	(0.0000, 0.0005)
MEK	145	80	10	0.6	(–0.0003, 0.0001)
MJ	180	56	45	0.8	(–0.0321, 0.0316)
NHY	154	77	–8	0.6	(0.0060, 0.1527)
PQ	70	75	–170	0.6	(–0.0002, 0.0014)
HY	150	75	45	0.6	(0.0007, 0.0033)
TZ	125	89	0	0.4	(–0.5296, 0.1044)
WM	205	60	142	0.6	(–0.0007, 0.0000)
WX	70	70	10	0.4	(0.0000, 0.0111)
YB	205	60	142	0.6	(–0.0004, 0.0006)

The fault parameters of NHY were defined as the mainshock fault inversed in this paper, with a friction of 0.6, the same as HY. The fault parameters of TZ were similar to the EK, considered as the southeastern extension of EK. The other fault parameters were from the Xu et al. [42]. The σ is the range of calculated Coulomb stress disturbances.

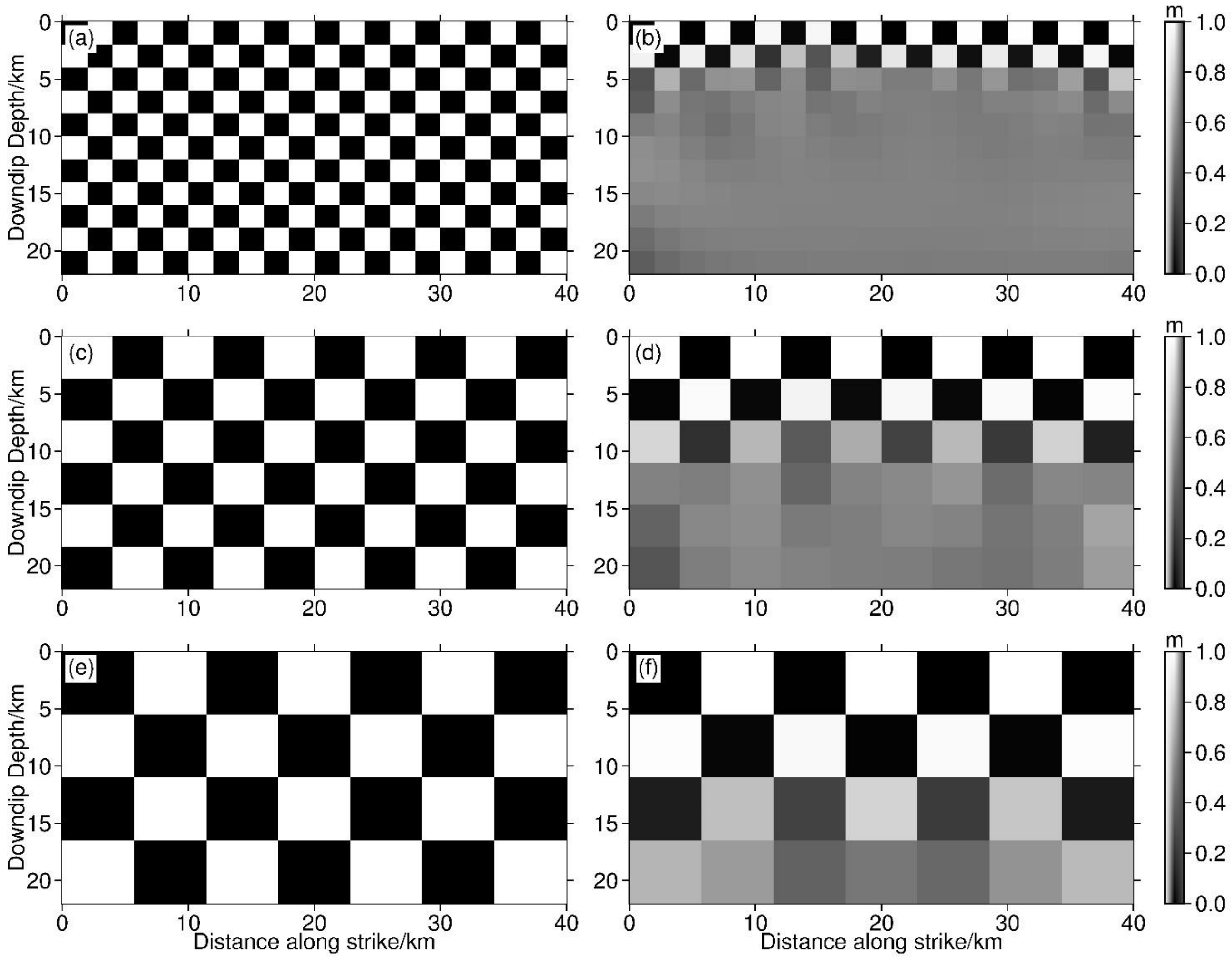

Figure S1. Checkerboard tests for the inversion of the InSAR and GPS data. (**a, c, e**) Input slip distribution with a patch size of 2 km, 4 km, and 6 km, separately; **(b, d, f**) Corresponding recovered slip distribution; this shows that the slip patch with 2 km, 4 km, and 6 km were well recovered at the downdip depth smaller than 4 km, 12 km, and 18km, separately.

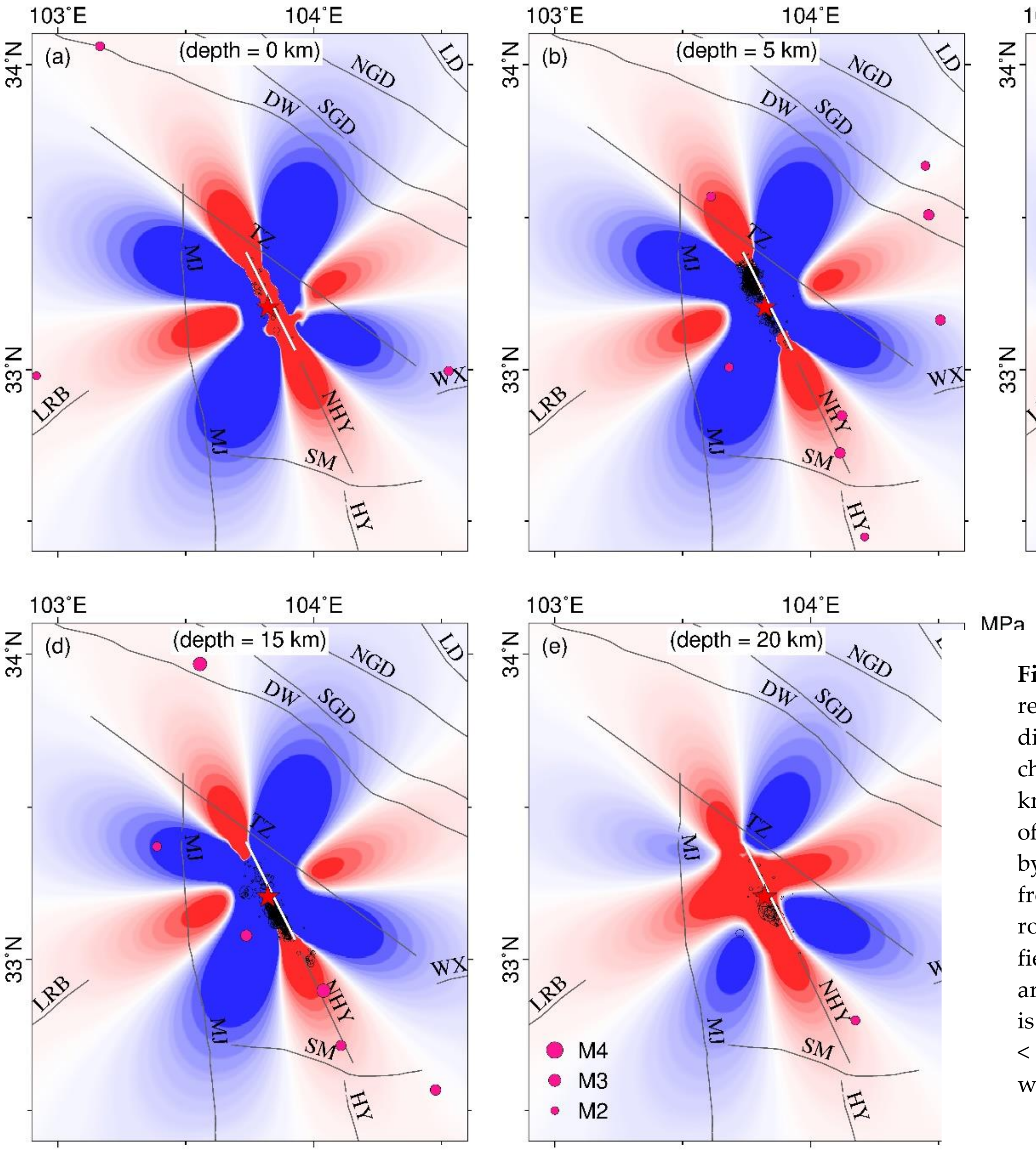

Figure S2. Coseismic Coulomb stress changes with the receiving fault of the mainshock rupture (i.e., strike = 154°, dip = 77°, rake = –8°, friction = 0.1). (**a**–**e**) Coulomb stress changes at the depths of 0 km, 5 km, 10 km, 15 km, and 20 km, respectively. The white line is the optimal fault model of this work. The near-field relocated aftershocks denoted by black circles and mainshock by the red pentagram are from Fang et al., [34]. The far-field aftershocks denoted by rose-red solid circles are from CSI. The magnitude of near-field aftershocks is referred to in Figure 9b. The gray lines are faults referred to in Figure 1. The depth of aftershocks is < 5 km with a, >= 5 km and < 10 km with b, >= 10 km and < 15 km with c, >= 15 km and < 20 km with d, and >= 20 km with e, respectively.

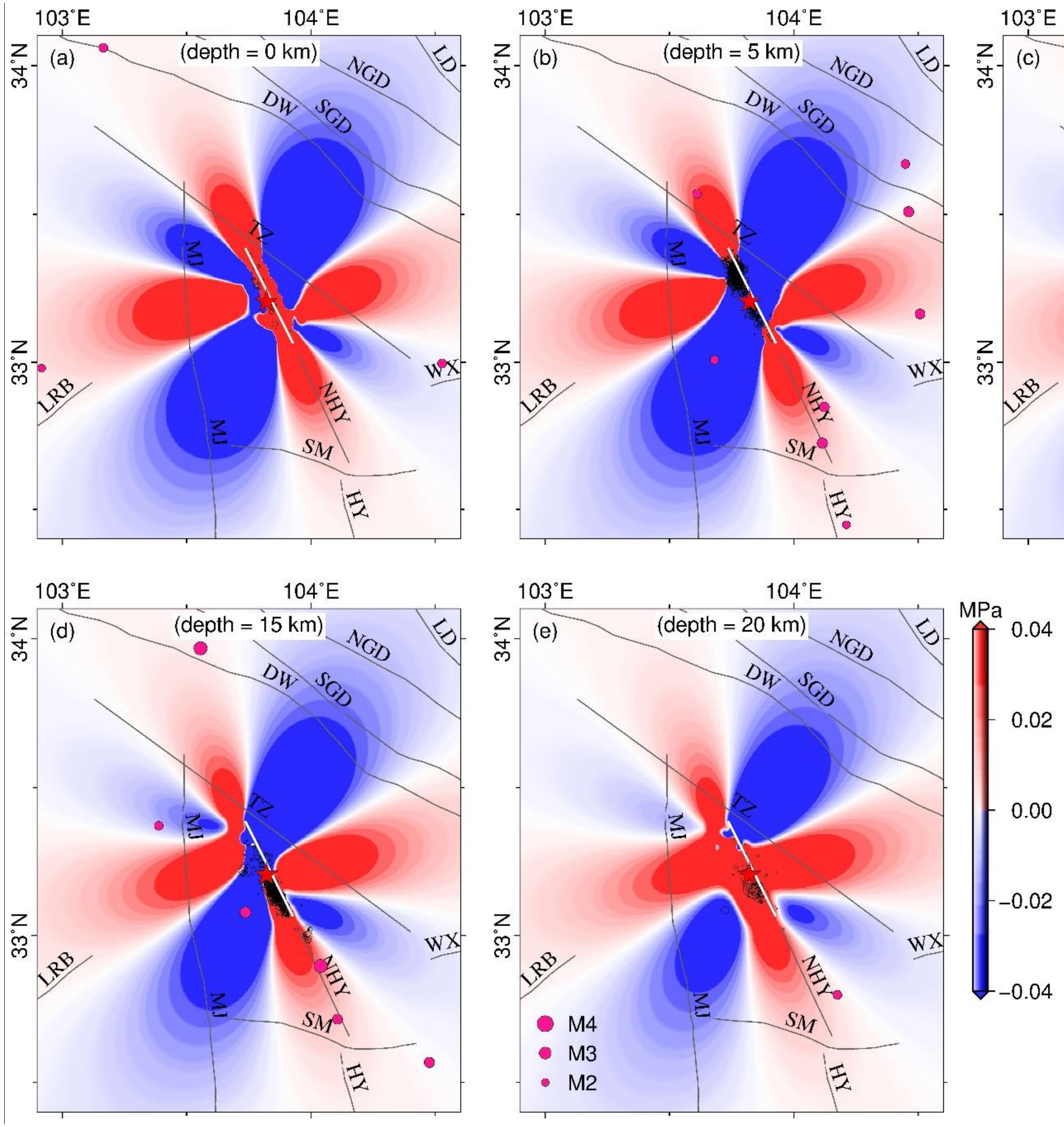

Figure S3. Coseismic Coulomb stress changes with the receiving fault of the mainshock rupture (i.e., strike = 154°, dip = 77°, rake = –8°, friction = 0.7). (**a**–**e**) Coulomb stress changes at the depths of 0 km, 5 km, 10 km, 15 km and 20 km, respectively. The white line is the optimal fault model of this work. The near-field relocated aftershocks denoted by black circles and mainshock by the red pentagram are from Fang et al., [34]. The far-field aftershocks denoted by rose-red solid circles are from CSI. The magnitude of near-field aftershocks is referred to in Figure 9b. The gray lines are faults referred to in Figure 1. The depth of aftershocks is <5 km with a, >=5 km and <10 km with b, >=10 km and <15 km with c, >=15 km and <20 km with d, and >=20 km with e, respectively.

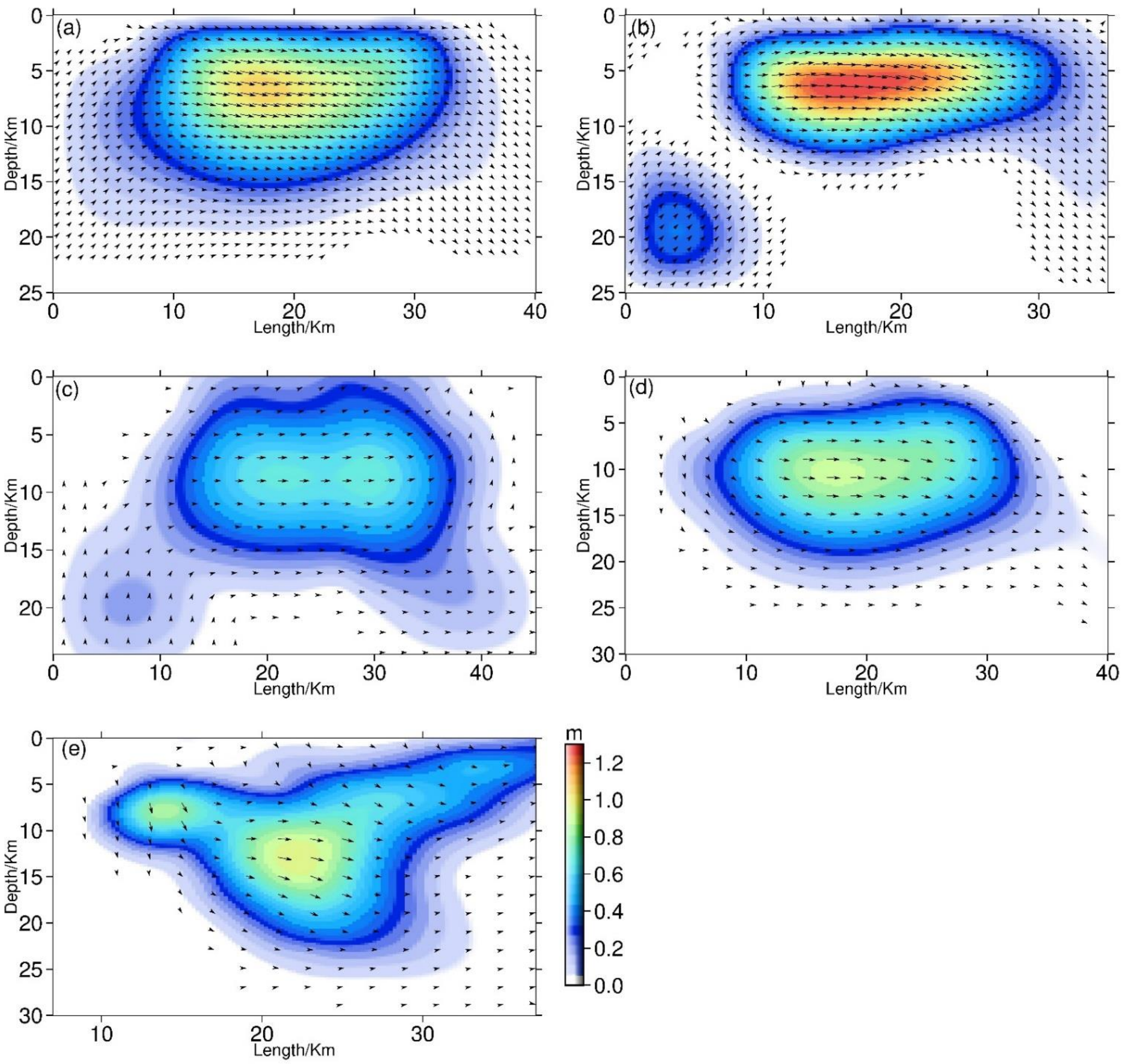

Figure S4. The comparison of our slip distribution model with the existing models. (a) Our fault slip model; (**b**–**e**) Fault sliding models with Zhao et al. [9], Ji et al. [7], Nie et al. [10], and Zhang et al. [12], respectively. The slip distribution models are in the same legend. The models of a, b, c, and d were retrieved by the geodetic data. The model e was derived by the geodetic and seismic waveform data.

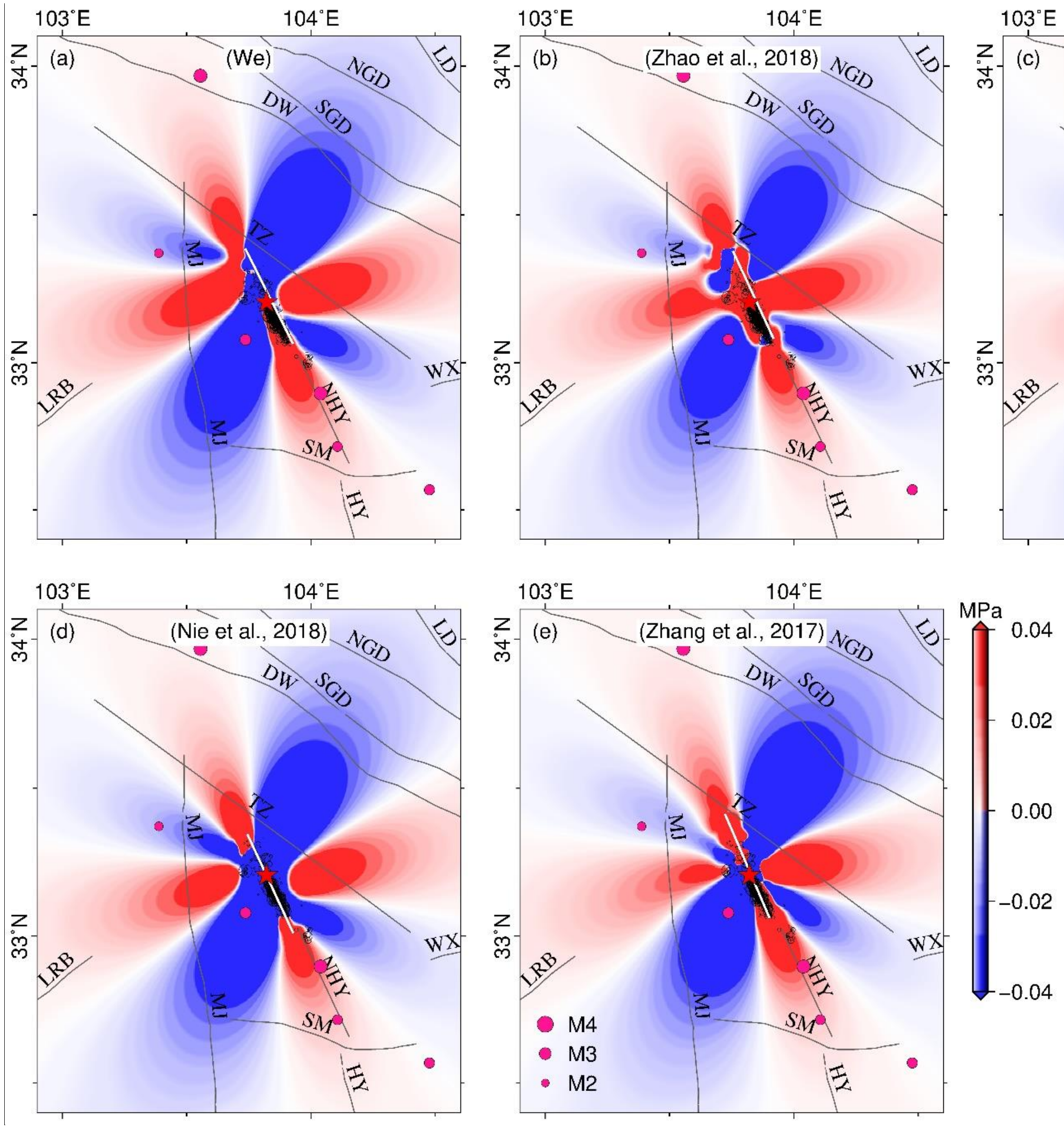

Figure S5. Coseismic Coulomb stress changes caused by the different slip models with the receiving fault of the mainshock rupture (i.e., strike = 154°, dip = 77°, rake = –8°, friction = 0.4) at the depth of 15 km. (**a**–**e**) Coulomb stress changes with the coseismic slip distribution models of this work, Zhao et al. [9], Ji et al. [7], Nie et al. [10], and Zhang et al. [12], respectively. The white lines are the fault models from the different researches. The relocated near-field aftershocks in the depths of 15–20 km denoted by black circles and mainshock by the red pentagram are referred to in Figure 10d. The gray lines are faults referred to in Figure 1. The far-field aftershocks within the depth of 15–20 km denoted by rose-red solid circles are from CSI.

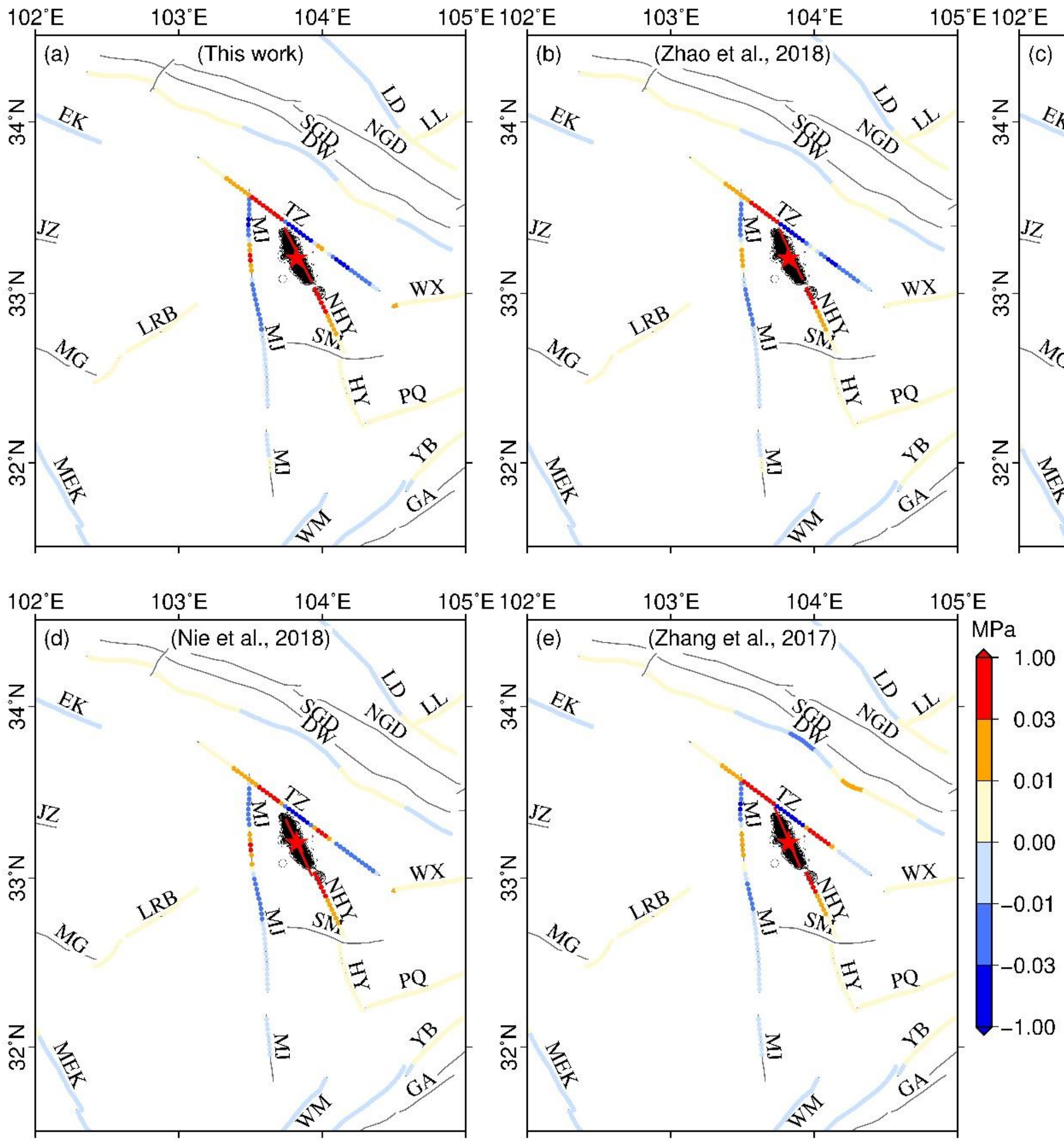

Figure S6. Static Coulomb stress disturbances caused by the different slip models with the same receiving fault (Table S1) at the depth of 5 km. (**a**–**e**) Static Coulomb stress changes with the coseismic slip distribution models of this work, Zhao et al. [9], Ji et al. [7], Nie et al. [10], and Zhang et al. [12], respectively. The red lines are the fault geometry models from the different studies. The relocated aftershocks denoted by black circles and mainshock by the red pentagram are referred to in Figure 11, and the magnitude of aftershocks are referred to in Figure 9b. The gray lines are faults referred to in Figure 1.